

Rotation misorientated graphene moiré superlattices on Cu(111): classical molecular dynamics simulations and scanning tunneling microscopy studies

P. Süle,¹ M. Szendrő,¹ C. Hwang,² and L. Tapasztó¹

¹*Research Centre for Natural Sciences, Institute for Technical Physics
and Materials Science Konkoly Thege u. 29-33, Budapest, Hungary*

²*Center for Nanometrology, Korea Research Institute of Standards and Science, Daejeon, Republic of Korea*
(Dated: February 27, 2022)

Graphene on copper is a system of high technological relevance, as Cu is one of the most widely used substrates for the CVD growth of graphene. However, very little is known about the details of their interaction. One approach to gain such information is studying the superlattices emerging due to the mismatch of the two crystal lattices. However, graphene on copper is a low-corrugated system making both their experimental and theoretical study highly challenging. Here, we report the observation of a new rotational moiré superlattice of CVD graphene on Cu(111), characterized by a periodicity of (1.5 ± 0.05) nm and corrugation of (0.15 ± 0.05) Å, as measured by Scanning Tunneling Microscopy (STM). To understand the observed superlattice we have developed a newly parameterized Abell-Tersoff potential for the graphene/Cu(111) interface fitted to nonlocal van der Waals density functional theory (DFT) calculations. The interfacial force field with time-lapsed classical molecular dynamics (CMD) provides superlattices in good quantitative agreement with the experimental results, for a misorientation angle of $(10.4 \pm 0.5^\circ)$, without any further parameter adjustment. Furthermore, the CMD simulations predict the existence of two non-equivalent high-symmetry directions of the moiré pattern that could also be identified in the experimental STM images.

keywords: graphene, moire patterns, superlattices, atomistic and nanoscale simulations, molecular dynamics simulations

I. INTRODUCTION

Chemical vapor deposition (CVD) on transition metal surfaces represents a promising and scalable approach to achieve reasonably uniform high-quality monolayer graphene for device applications^{1–3}. Polycrystalline copper foils have widely been used as substrate for the CVD growth of graphene^{3,4}. On the other hand the Cu(111) facet has been proposed as one of the preferred surfaces for the large-scale uniform high-quality monolayer graphene growth⁵. The characterization and interpretation of various graphene (gr) superstructures, such as the moiré supercells^{6,7} and the corresponding nanoscale topography requires sophisticated experimental and theoretical methods^{8–10}. Recent studies show that weakly adhered graphene on various substrates exhibits multiple oriented rotated moiré regions with different misorientation angles^{5,11–21}.

In systems with stronger adhesion (e.g. gr/Ru(0001)) the appearance of rotated moire superstructures is still under debate^{10,16,22,23}. In a recent study it has been shown that the moiré hills (called moirons) are nonequivalent and therefore the large coincident supercell is the unit cell of moiré patterning in gr/Ru(0001)¹⁰ confirmed by other experimental works²². Even in rigid lattice approximation in coincident supercells lattice missfit van-

ishes and this superlattice can be taken as the unit cell of moiré patterning²⁴. The graphene overlayer often exhibits an additional longer range topographic modulation, besides the apparent periodicity, when local geometric distortions are considered (buckling, local lateral distortions and/or lattice rotation)²⁴.

It has also been shown that a few types of rotated moiré patterns could coexist in gr/Pt(111) and gr/Ir(111). In gr/Cu(111) the occurrence of rotated gr grains is much less studied⁵ as compared to other substrates such as Ir(111), Pt(111), Ni(111), which can be attributed to the imaging difficulties in this important low-corrugated system with large repeat distance^{5,12}. Until now, two types of rotated domains have been identified: one with nearly vanishing rotation angle Θ (denoted as R0) and large moiré supercells (the cell size is around 6 nm) and another with $\Theta \approx 7^\circ$ (R7) with a much smaller periodicity of ~ 2 nm^{5,11,12}. A bump-to-hump corrugation of $\xi \approx 0.35$ Å has been measured by STM for the aligned gr/Cu(111)¹¹. For rotation misoriented samples no corrugation data is available.

In this paper we show that another rotated phase can also exist on Cu(111) with so far the smallest periodicity of 1.5 nm and the largest rotation angle of 10.4° (R10). Experimental (STM) and theoretical classical molecular dynamics (CMD) methods have been employed to characterize the new rotated phase. A new CMD force field is developed for gr/Cu(111) to analyze the moiré superstructures in atomic detail and the height variation is measured by STM along different symmetry directions of the gr/Cu(111) system. It has been shown recently that

¹ Corresponding author E-mail: sule@mfa.kfki.hu (Péter Süle)

² Corresponding author tel.: +361392222/1909 (Péter Süle)

TABLE I: The fitted Abell-Tersoff parameters for the graphene/Cu(111) interface.

C-Cu	
A (eV)	977.7958178
B (eV)	320.7794950
λ_1	3.1308174
λ_2	2.0455965
γ	0.0883168
c	40.9755961
d	0.9528753
h	0.9050528
R_c (Å)	4.1978605
D_c (Å)	0.4794477
β (Å ⁻¹)	1.0
λ_3	1.5527866
n,m	1

^aThe parameters have been fitted to small flat gr/Cu(111) systems. Notations are the same as used in ref.²⁶ (supplementary material) and on the web page of lammmps³⁷. λ_3 is denoted as μ and $h = \cos\theta_0$ in the supplementary material of ref.²⁶.

the development of a new interfacial force field provides the adequate description of the prototypical gr/Ru(0001) system²⁶. First principles calculations (such as DFT) have widely been used in the last few years to understand the corrugation of nanoscale gr sheets on various substrates^{8,9,27,28}, modelling larger systems, above 1000 carbon atoms remains, however challenging, especially when geometry optimization is included. The minimal supercell of the gr/Cu(111) system includes a few thousands of carbon atoms which definitely exceeds the size limit of accurate DFT geometry optimizations and/or *ab initio* DFT molecular dynamics. Here we show that using a new DFT adaptively parameterized interfacial Abell-Tersoff potential^{29,30} one can quantitatively reproduce even the fine structure off the experimentally observed surface reconstructions of gr on Cu(111) (moiré superstructures).

II. METHODOLOGY

A. STM setup

Scanning tunneling microscopy (STM) is one of the most suitable characterization tools for studying moiré-superlattices of graphene emerging due to the mismatch of the atomic lattices of graphene with various substrates. This is mainly due to its high (atomic) resolution capability and the ability to reliably detect extremely small height variations, provided that the variation of the local density of states (LDOS) is negligible as compared to topographic features. However, a significant redistribution of the LDOS affecting the corrugation measured by STM is only expected for high (nanometer radius) local curvatures of graphene membranes and particularly strong substrate interactions (e.g. graphene on Ru, Ni).

STM investigations have been successfully employed to investigate moiré-patterns emerging in graphene on Ru(0001)³¹, Ir(111)³², Rh(111)³³ as well as in nonmetallic substrates such as 6H-SiC(0001)³⁴ and h-BN³⁵. For the case of graphene on Cu(111), neither the curvature, nor the substrate interaction is strong enough to substantially alter the local electronic density of states distribution; consequently, the measured image is expected to be of topographic origin. This is confirmed by the fact that the measured corrugation was not sensitive to the applied bias voltage.

Our STM measurements have been performed at low temperature (78 K) and under UHV conditions. The investigated graphene samples were grown on polished Cu(111) single crystal surfaces by Chemical Vapor Deposition at 990 C° and 1250 mtorr base pressure, using a methane/hydrogen (20sccm:5sccm) gas mixture as precursor. After growth the samples have been transferred into the UHV system. No annealing of the sample was necessary prior to STM measurements.

B. Simulation rules

Classical molecular dynamics has been used as implemented in the LAMMPS code (Large-scale Atomic/Molecular Massively Parallel Simulator)³⁷. The graphene layer has been placed commensurately on the substrate since the lattice mismatch is small in gr/Cu(111). However, even this tiny misfit is sufficient to form partly registered positions (alternating hexagonal hollow and ontop sites) which leads to a moiré superstructure.

Periodic triclinic (rhombohedral) simulations cells have been constructed with 85×85 and 255×255 gr-unit cells. We find these structures to be suitable for simulations leading to commensurate superstructures. The systems are carefully matched at the cell borders in order to give rise to perfect periodic superstructures. Arbitrary system sizes lead to non-perfect matching at the borders. Moreover, nonperiodic cells lead to unstable moiré patterns due to the undercoordinated atoms at the system border which cannot be handled by the present force field with CMD. Nonperiodic structures can be, however, optimized by simple minimizers which also provide moiré patterns. Further refinement of the pattern can be obtained by time-lapsed CMD. The moiré pattern is extremely sensitive to weak effects during CMD such as e.g. the improperly treated border atoms and/or the arising tensile stress or strain at the simulation cell border.

Isobaric-isothermal (NPT ensemble) simulations (with Nose-Hoover thermostat and a prestostat) were carried out at 78 K (STM measurements were also performed at this temperature). Vacuum regions were inserted between the slab of the gr-substrate system to ensure the periodic conditions not only in lateral directions (x,y) but also in the direction perpendicular to the gr sheet (z). The variable time step algorithm has been exploited.

The codes OVITO³⁸ and Gnuplot has been utilized for displaying atomic and nanoscale structures^{26,39}.

The molecular dynamics simulations allow the optimal lateral positioning of the gr layer and the minimization of the lattice misfit. The relaxation of the systems has been reached in 3 steps: first conjugate gradient geometry optimization (cg-min) with a subsequent simulation box relaxation (boxrel) of the rhomboid simulation cell has been carried out. Finally variable time step CMD simulations have been utilized in few tens of a thousand simulation steps to allow the further reorganization of the system under thermal and pressure controll (NPT, Nose-Hoover thermostat, prestostat). Therefore we use in general the combined cg-min/CMD simulations. Time-lapsed CMD (TL-CMD) has been used at 78 K in order to average the morphology over longer timescale and also to account for the effect of temperature. We found that 10000 steps are generally sufficient for a stable moiré pattern. The pattern remains stable for time averages of much longer simulations.

The AIREBO (Adaptive Intermolecular Reactive Empirical Bond Order) potential has been used for the graphene sheet⁴⁰. For the Cu substrate, a recent embedded atomic method (EAM)⁴¹ potential is employed. For the C-Cu interaction we developed a new Abell-Tersoff-like angular-dependent potential³⁰ (this potential goes beyond the level of pairwise interactions and bond angle dependence has also been explicitly included). In the Abell-Tersoff potential file (lammmps format) the C-C and Cu-Cu interactions are ignored (nulled out). The CCuC and CuCCu out-of-plane bond angles were considered only. The CuCC and CCuCu angles (with in-plane bonds) are ignored in the applied model. Considering these angles requires the specific optimization of angular parameters which leads to the polarization of angles that does not fit to the original Abell-Tersoff model.

C. Parameter fitting

We used typical small gr/Cu(111) configurations (with flat graphene sheet) representatives for binding registries of hollow, top-fcc, top-hcp and bridge alignments (see e.g. ref.²⁶). The potential energy curve (PEC) of the rigid gr-Cu(111) separation has been calculated by non-local VdW-DFT⁴² using the SIESTA code⁴³. Then using a code developed by us⁴⁴ the interfacial Abell-Tersoff potential has been fitted to these DFT PECs. The following conditions had to be satisfied by the parameter set: (i) minimal rhomboid supercell edge size ($d \approx 6.1$ nm) for flat aligned gr (ii) proper topology of the gr-surface: hump-and-bump morphology with a corrugation of $\xi \approx 0.35 \pm 0.05$ Å. Hollow-humps (moiré hills) and ontop-bumps (wells) are required as it has been found in other gr/substrate systems (e.g. gr/Ru(0001)²⁶). (iii) interface energy: adsorption or adhesion energy $E_{adh} \approx 0.11 \pm 0.02$ eV/atom (iv) correct interfacial distances: $d_{C-Cu} \approx 3.1 \pm 0.1$ Å. Among these requirements we im-

posed directly only conditions (iii) and (iv) under parameter fitting (corrugation has not directly been included in the parameter fitting set). However, the new parameter set also satisfied automatically conditions (i)-(ii). Conditions (iii)-(iv) seem to be sufficiently strict to restrict the parameter space in order to account for the morphology, structure and energetics of the moiré superstructures of gr/Cu(111). The obtained parameter set is shown in Table I. A more detailed technical discussion of parameter fitting can be found in Ref.⁴⁵.

D. *Ab initio* DFT calculations

First principles DFT calculations have also been carried out for calculating the adhesion energy per carbon atoms vs. the C/Cu distance for a small ideal system with a flat graphene layer. The obtained PECs can be compared with the similar curve of MD calculations. We also calculate the DFT potential energy curves of various binding registries of gr including the hollow and on-top configurations (atop-fcc and hcp) and also the bridge one.

For this purpose we used the SIESTA code^{43,46} which utilizes atomic centered numerical basis set. The SIESTA code and the implemented Van der Waals functional (denoted as DF2, LMKLL in the code⁴⁶) successfully employed in several cases for gr (see e.g. recent refs.^{47,48}). We have used Troullier Martin, norm conserving, relativistic pseudopotentials in fully separable Kleinman and Bylander form for both carbon and Cu. A double- ζ polarization (DZP) basis set was used. In particular, 16 valence electrons are considered for Cu atoms and 4 for C atoms. Only Γ point is used for the k-point grid in the SCF cycle. The real space grid used to calculate the Hartree, exchange and correlation contribution to the total energy and Hamiltonian was 300 Ry (Meshcutoff).

III. RESULTS AND DISCUSSION

The STM images shown in Fig. 1(a) and (b) reveal an unexpected rotation-misoriented phase with a periodicity of (1.5 ± 0.05) nm that has not been reported so far. The STM images in Fig. 1(a) and (b) have been acquired at low temperature (78K) using a bias voltage of -230 mV and 5 nA tunneling current, under UHV conditions. From Fig 1(b) the periodicity of the honeycomb lattice has been removed by Fourier filtering, to better visualize the details of the moiré pattern. The observed periodicity is the smallest graphene superlattice reported on Cu (111) so far. The new moiré phase has been observed in several locations on two different samples.

We found that a larger-angle rotated moiré superstructure ($\Theta \approx 10.4^\circ$) is able to reproduce our STM findings reported here (see Figs 1(a)-(b)). The corresponding CMD results can be seen in Figs 1(c)-(d). Until now there are only a few experimental works reporting a ro-

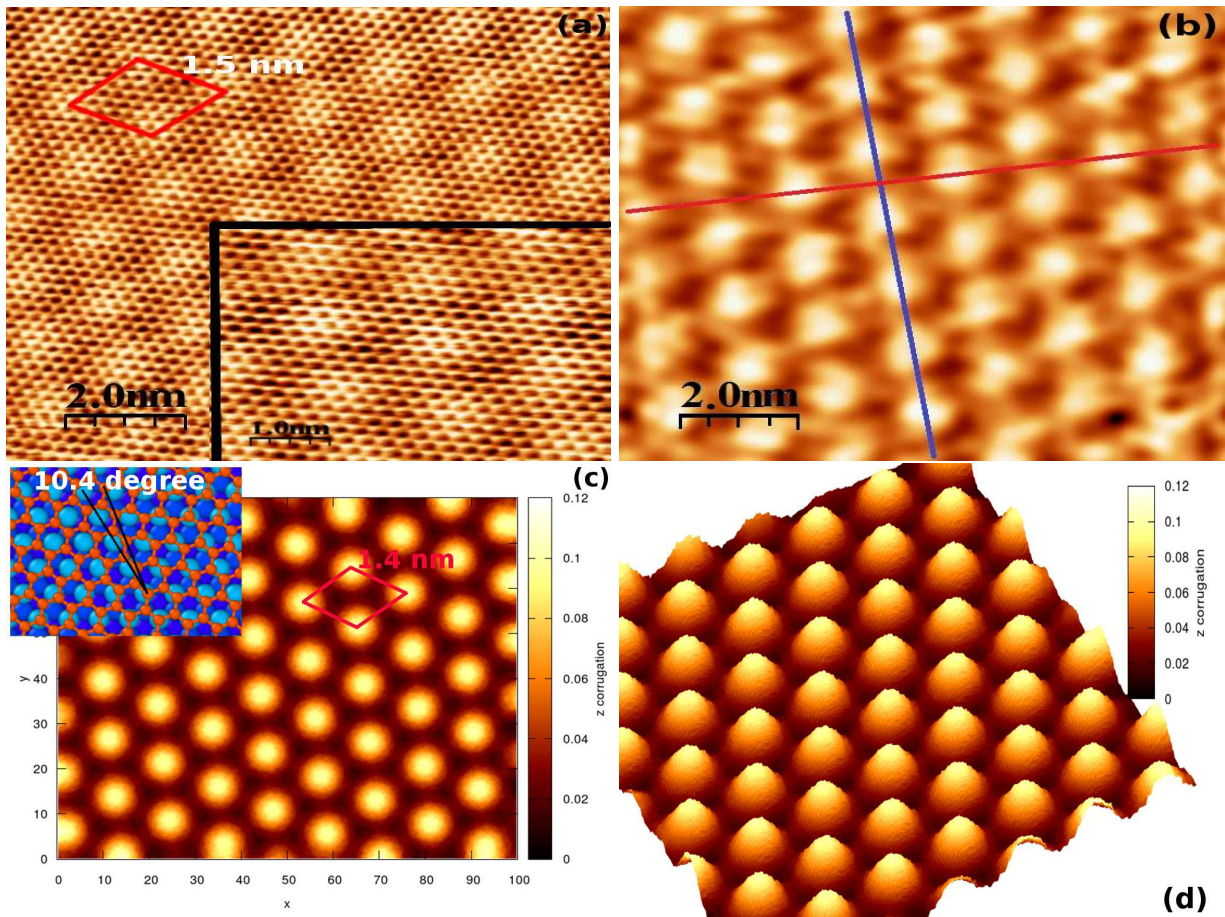


FIG. 1: The results of STM measurements and CMD simulations on graphene/Cu(111) moiré superstructures at the rotation angle of $\Theta \approx 10.5 \pm 0.5^\circ$. (a)-(b) Experimental STM images displaying moiré superlattice with atomic resolution (a) and when the atomic corrugation has been removed by Fourier filtering to make the details of the superlattice more apparent. (b) The directions for measuring the height profiles are also shown (along the long (red) and short (blue) diagonal of the rhombic supercell). In the Inset of (a) a magnified image is also shown. (c) Simulated topographic image. The x,y axes and the corrugation are given in Å. The minimal (1×1) supercells is also shown with a red rhombus. *Inset*: The measured rotation angle in the CMD simulations (the angle between the zig-zag line of carbon atoms and the line of (110) Cu atoms). (d) CMD simulated height profile (3D image) with the moiré humps (protrusions). Corrugation is given in Å.

tated phase of graphene on Cu(111). One reported rotated phase is of $\Theta \approx 7^\circ$ (R7) with the periodicity of $d_{per} \approx 2 - 2.2$ nm^{5,12}. Our misoriented phase occurs at considerably larger angle implying a smaller repeat distance. In particular, we found ($d_{per} \approx 1.5 \pm 0.05$) nm (STM) and the substantial drop of corrugation with respect to $\Theta \approx 0^\circ$ ($\xi \approx 0.012$ nm). We denote this phase as R10. CMD simulations give a slightly smaller $d_{per} \approx 1.4 \pm 0.05$ nm. This difference can be due to the experimental error. Therefore we propose that a novel stable rotational phase has been identified both theoretically and experimentally.

The height variation of gr along different directions can be seen on Figs. 2(a)-2(d). Concerning the larger-angle rotated sample R10 ($\Theta \approx 10.4^\circ$), two main sections are shown along high symmetry directions of the superlattice. On Figs. 2(a)-(b) the height profiles are

seen along the short diagonal of the minimal rhomboid supercell from CMD simulations (2(a)) and from STM (2(b)). Figs. 2(c)-(d) depict the long diagonal height profiles for CMD simulations (2(c)) and the corresponding STM cross section(2(d)). The most striking features are the small satellite peaks in between the main moiré hills, observed in both the measured and simulated cross sections. The splitting of the height profiles along distinct directions for gr moiré patterns has also recently been reported for gr/Ir(111)²⁵. The corrugation for the rotated patterns remains below 0.015 nm for both directions, while the corrugation of the small satellite peaks is of just 0.005 nm.

The observed moiré superstructure has been reproduced and characterized by CMD simulations (Figs 1(c)-(d)) which required, however, the development of a new interfacial force field. Using this method we could also

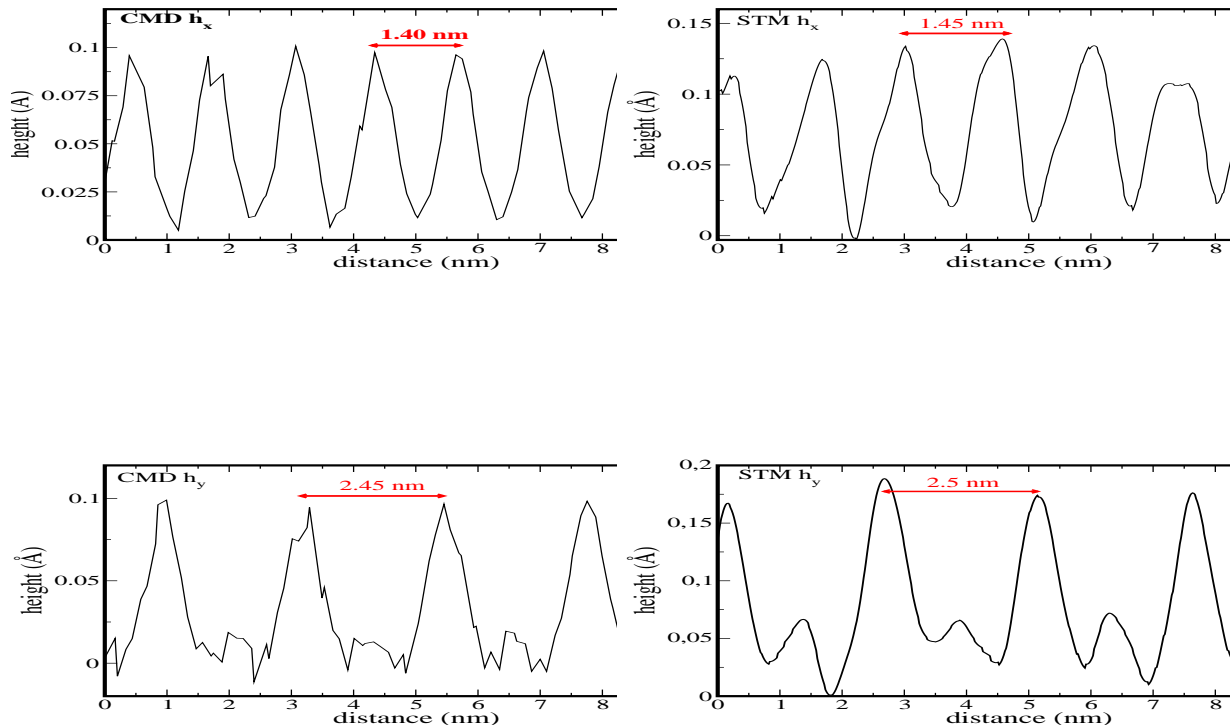


FIG. 2: Height profiles in the R10 phase along the two high symmetry directions, cut out within thin sections with the thickness of 2 Å, as obtained by CMD (a) and by STM (b) along the shorter diagonal of the rhomboid supercell (along the blue line, in Fig 2(d)). The repeat distances d_{per} are also shown. (c)-(d): Height profiles along the longer diagonal of the supercell as obtained by: CMD (c) and by STM (d) (along the red line in Fig 2(d)). Note that the secondary peaks between the moiré peaks can also be seen.

identify the two reported phases R0 and R7 phase reported in refs.^{5,12} by cg-min/CMD simulations. Moreover, our simulations predict the existence of several other stable rotated phases, such as R2, R9 and R16 which have not been observed yet. In particular, the angular dependent Abell-Tersoff potential³⁰ has been used for the interface which was fitted to nonlocal vdW-DFT potential energy curves of small model systems with hcp and hollow binding registries. No explicit information has been used in the fitting procedure on corrugation, supercell size or other experimentally measured quantities to be accounted for²⁶. The new potential together with the AIREBO⁴⁰ C-C potential on Cu(111) is capable of reproducing the moiré superstructures seen by STM^{5,11} at nearly zero misorientation angle. The obtained periodicity (d_{per}) of the small supercell is 6.1 nm in accordance with the experiments^{5,11}. The resulting corrugation of $\xi \approx 0.4$ Å, is also in agreement with the available STM data¹¹. We could also reproduce by CMD simulations the R7 ($\Theta \approx 6.7^\circ$) phase with a somewhat larger repeat

distance of $d_{per} \approx 2.5 \pm 0.05$ nm than found by STM in recent publications (2.0 – 2.2 nm,^{5,12}).

In general we report the rapid decrease of the repeat distance with rotation angle, for instance for $\Theta = 16^\circ$ the value of $d_{per} \approx 0.88$ nm has been found by CMD simulations (see Table II.). We could not identify stable phases with larger rotation angle with CMD.

In Table II. the various structural and energetic properties of the simulated rotated structures have been summarized. The notable features are the following: corrugation decreases with Θ and practically vanishes for $\Theta > 15^\circ$. The lattice constant of the gr sheet shows no considerable sensitivity to Θ and is stabilized at $a_{gr} \approx 2.44$ Å (the gr lattice is slightly compressed).

In spite of the significant lattice misfit of $a_{lm} < 3.56$ % the aligned gr $\Theta \approx 0^\circ$ phase is very close in energy to that of the perfectly relaxed flat gr, with a vanishingly small energy difference ($\Delta E \approx 0.007$ eV/C) although its corrugation is significant ($\xi \approx 0.45$ Å). This can be attributed to the strain relief in the large coincidence

TABLE II: The summary of various properties obtained for gr/Cu(111) by classical molecular dynamics simulations using the fitted Abell-Tersoff potential for the interface. The main properties of the moiré superstructures.

method	Θ	d_{per} (nm)	ξ (Å)	ξ_{Cu} (Å)	d_{ave} (Å)	a_{gr} (Å)	a_{lm} (%)	E_{adh} (eV/C)	ΔE	E_{gr}
CMD	0.0° (R0)	6.1	0.45	0.1	2.99	2.440	3.56	-0.146	0.0072	-7.419
	2.2° (R2)	4.3	0.25	0.1	2.99	2.440	3.56	-0.146	0.04	-7.384
	6.7° (R7)	2.5	0.14	0.06	3.02	2.445	3.44	-0.145	0.035	-7.391
	8.7° (R9)	1.75	0.12	0.05	3.02	2.445	3.44	-0.145	0.02	-7.406
	10.4° (R10)	1.4	0.1	0.05	2.99	2.440	3.70	-0.145	0.04	-7.385
	16.1° (R16)	0.88	0.03	0.02	3.02	2.444	3.56	-0.145	0.04	-7.385
EXP	$\sim 0^\circ$ (R0)	6.0 ^a	0.35 ± 0.1^a	n/a	n/a	2.46	3.53	-0.11 ^b	n/a	n/a
	7° (R7)	2.0 ^c , 2.2 ^d	n/a	n/a	n/a	n/a	n/a	n/a	n/a	n/a
	10.4° (R10), pw ^e	1.5	0.15 ± 0.05	n/a	n/a	n/a	n/a	n/a	n/a	n/a
DFT	0°	n/a	n/a	n/a	3.25 ^f , 3.05 ^g	n/a	n/a	-0.062 ^f , -0.198 ^g	n/a	n/a

[1] dimensions: Å has been used for corrugation and nm for the periodicity. pw denotes present work, Θ is the rotation angle in degree (the angle between the line of zig-zag carbon atoms and the adjacent Cu(111) atoms along the line (110) shown in Inset Fig 1(c)). d_{per} is the periodicity of the minimal moiré pattern (the edge length of the rhombus with 4 moiré humps, 1×1 supercell), ξ and ξ_{Cu} are the average corrugation for gr and the topmost Cu(111) layer (Å). d_{ave} is the average inter-layer (C-Cu) distance (Å) at the interface. a_{gr} , a_{lm} are the lattice constant of gr (Å) and the lattice mismatch (%) after simulations ($a_{lm} = 100(a_s - a_{gr})/a_{gr}$). CMD: pw, fitted Abell-Tersoff results with cg minimization with CMD at 300 K. EXP: the experimental results: corrugation (ξ): our STM results, DFT results are also given for comparison^{6,9,28}. All quantities are given per carbon atom. The adhesion energy $E_{adh} = E_{tot} - E_{no12}$, where E_{tot} is the potential energy/C after CMD simulation. E_{no12} can be calculated using the final geometry of CMD simulation with heteronuclear interactions switched off. Therefore, E_{adh} contains only contributions from interfacial interactions. $E_{str,gr}$, the strain energy of the corrugated gr-sheet, ΔE (eV/C) is the energy difference with respect to the perfectly flat periodic gr. $\Delta E = E_{gr} - E_{gr,flat}$, where E_{gr} and $E_{gr,flat} = -7.426$ eV/C are the cohesive energy of C atoms in the corrugated and in the relaxed periodic flat (reference) gr sheet as obtained by the AIREBO C-potential⁴⁰. ^a from refs.^{5,11}, ^b from ref.⁵¹, double cantilever beam method: $E_{adh}=0.72$ J/m². ^c from ref.¹¹, ^d from ref.¹², ^e present STM work, ^f from ref.⁵², obtained by accurate random phase approximation for a very small model system. ^g present work: nonlocal vdw-DFT calculation for a small flat system (463 atoms): hcp: -0.198 eV/C ($d_0 = 2.95$ Å), hollow: -0.182 eV/C ($d_0 = 3.09$ Å), vdw-DFT geometry optimized structures: ontop hcp: -0.350 eV/C, hollow: -0.133 eV/C.

*

supercells¹⁰. We found 0.16 % lattice mismatch in the minimal supercell in the R0 phase. In the case of the mis-oriented phase reported here with $\Theta = 10.4^\circ$ the misfit of the coincidence supercells are 1.47 % for the minimal supercell (red rhombus in Figs 1(a) and (b)).

Concerning the energetic stability with respect to the perfectly flat periodic gr, $\Delta E \approx 0.04$ eV/C (see Table II.) which is somewhat above the magnitude of thermal motion (~ 0.026 eV/K at 300 K) which in principle renders this phase detectable even at room temperature. Also the energy difference between the aligned and the rotated phase ($\Theta = 10.4^\circ$) is in similar range ($\Delta E \approx 0.033$ eV/C).

Interestingly, the large angle rotation ($\Theta > 15^\circ$) also does not require much more energy ($\Delta E \approx 0.04 - 0.05$ eV/C). This suggests that at elevated temperatures, however, (few hundred K above room temperature) the complexity of the multiple-oriented rotation domains could be increased significantly and the number of the large angle rotated regions could be considerable. This clearly

indicates that the high temperature conditions (1200 K) of CVD growth of gr could be sufficient for the occurrence of a large variety of large angle rotational domains. The pinning of various rotated domains, once formed during CVD growth could occur. Therefore, we predict the coexistence of various misaligned gr moiré patterns including ultraflat (highly rotated), low-angle rotated and aligned regions (corrugated) which are energetically permitted. It must be noted that the large angle rotated domains ($\Theta > 15^\circ$), do not show moiré patterns due to the vanishing corrugation and small repeat distance. Similar findings have been reported for gr/Ir(111)⁴⁹ at much larger rotation angles of 30° while the corrugation was 10 times smaller than for the aligned phase. Considering that the morphology of gr/Cu(111) is rich even without rotation⁵⁰ it is not easy to directly assign a rotation angle to an observed moiré superlattice. Recent studies suggest similar findings for gr/Pt(111)¹⁵ or for gr/Ir(111)¹⁷.

The *adhesion energy* has also been calculated and is

shown for various rotated superlattices in Table II. We find a somewhat larger adsorption energy of -0.145 eV/C than by experiment (-0.11 eV/C,⁵¹). In general, the binding energy of gr to Cu(111) is smaller than in other systems, such as gr/Ru(0001) ($0.17 - 0.2$ eV/C, see e.g. ref.²⁶) and larger than in the weakest bound systems (e.g. gr/SiO₂, $E_{adh} \approx -0.07$ eV/C)⁵³. No considerable dependence of E_{adh} has been found on Θ .

IV. CONCLUSIONS

We have developed a new interfacial force field to describe various moiré superstructures emerging in graphene on Cu(111) surface. No such interface interaction potential, adequately describing the moiré superlattices of graphene/Cu(111) interface has been available so far. Using classical molecular dynamics simulations we have shown that our method can provide reasonably accurate structural results even for weakly bound (low-corrugated) extended systems such as graphene on copper. We also report the experimental observation of a

new rotated phase of 1.5 nm periodicity, that has not yet been observed experimentally. Using the new potential we have successfully reproduced the observed novel phase for rotation angle of 10.4° , including the fine structure of the superlattice, without any further parameter adjustment. Furthermore, our model predicts the existence of various superlattices. Interestingly, while aligned and low-angle rotated structures display a clearly detectable corrugation, further increasing the misalignment quickly flattens the graphene sheet. Angles larger than 15° are predicted to yield ultra-flat graphene.

V. ACKNOWLEDGEMENT

LT and CH acknowledges financial support from the Korea Hungary Joint Laboratory for Nanosciences and OTKA grant K 108753. The calculations (simulations) have been done mostly on the supercomputers of the NIIF center (Hungary). The availability of codes LAMMPS (S. Plimpton) and OVITO (A. Stukowski) are also greatly acknowledged.

-
- ¹ Z. Z. Sun, Z. Yan, J. Yao, E. Beitler, Y. Zhu, J. M. Tour, Growth of graphene from solid carbon sources, *Nature*, **468**, 549 (2010).
 - ² K. S. Kim, Y. Zhao, H. Jang, S. Y. Lee, J. M. Kim, *et al.*, Large-scale pattern growth of graphene films for stretchable transparent electrodes, *Nature*, **457**, 706 (2009)
 - ³ Y. Hao, M. S. Bharathi, L. Wang, Y. Liu, H. Chen, S. Nie, X. Wang, H. Chou, C. Tan, B. Fallahazad, H. Ramakrishnan, C. W. Magnuson, E. Tutuc, B. I. Yakobson, K. F. McCarty, Y.-W. Zhang, P. Kim, J. Hone, L. Colombo, R. S. Ruoff, The Role of Surface Oxygen in the Growth of Large Single-Crystal Graphene on Copper, *Science*, **342**, 720. (2013).
 - ⁴ X. Li, W. Cai, J. An, S. Kim, J. Nah, D. Yang, R. Piner, A. Velamakanni, I. Jung, E. Tutuc, S. K. Banerjee, L. Colombo, R. S. Ruoff, Large-Area Synthesis of High-Quality and Uniform Graphene Films on Copper Foils, *Science* **324**, 1312. (2009).
 - ⁵ L. Gao, J. R. Guest, and N. P. Guisinger, Epitaxial Graphene on Cu(111), *Nano Lett.* **10**, 3512. (2010).
 - ⁶ M. Batzill, *The surface science of graphene: Metal interfaces, CVD synthesis, nanoribbons, chemical modifications, and defects*, Surface Science Reports, **67**, 83. (2012).
 - ⁷ J. Wintterlin, M.-L. Bocquet, *Graphene on metal surfaces*, Surf. Sci. **603**, 1841-1852 (2009).
 - ⁸ D. Stradi, S. Barja, C. Daz, M. Garnica, B. Borca, J. J. Hinarejos, D. Sanchez-Portal, M. Alcami, A. Arnau, A. L. Vazquez de Parga, R. Miranda, and F. Martin, Role of Dispersion Forces in the Structure of Graphene Monolayers on Ru Surfaces, *Phys. Rev. Lett.* **106** 186102 (2011).
 - ⁹ M. Iannuzzi, J. Hutter, Comparative study of the nature of chemical bonding of corrugated graphene on Ru(0001) and Rh(111) by electronic structure calculations, *Surf. Sci.*, **605** 1360 (2011).
 - ¹⁰ M. Iannuzzi, I. Kalichava, H. Ma, S. J. Leake, H. Zhou, G. Li, Y. Zhang, O. Bunk, H. Gao, J. Hutter, P. R. Willmott, and T. Greber, Moiré beatings in graphene on Ru(0001), *Phys. Rev.* **B88** 125433 (2013).
 - ¹¹ L. Zhao, K. T. Rim, H. Zhou, R. He, T. F. Heinz, A. Pinczuk, A., G. W. Flynn, A. N. Pasupathy, Solid State Commun. **151**, 509. (2011), W. Kim, K. Yoo, E. K. Seo, S. J. Kim, C. Hwang, Scanning Tunneling Microscopy Study on a Graphene Layer Grown on a Single-crystal Cu(111) Surface by Using Chemical Vapor Deposition, *J. Korean Phys. Soc.*, **59**, 71. (2011).
 - ¹² T. Niu, M. Zhou, J. Zhang, Y. Feng, and W. Chen, Growth Intermediates for CVD Graphene on Cu(111): Carbon Clusters and Defective Graphene, *J. Am. Chem. Soc.*, **135**, 8409 (2013).
 - ¹³ R. He, L. Zhao, N. Petrone, K. S. Kim, M. Roth, J. Hone, P. Kim, A. Pasupathy, and A. Pinczuk, Large Physisorption Strain in Chemical Vapor Deposition of Graphene on Copper Substrates, *Nano Lett.*, **12** 2408. (2012).
 - ¹⁴ S. Nie, J. M. Wofford, N. C. Bartelt, O. D. Dubon, K. F. McCarthy, Origin of the mosaicity in graphene grown on Cu(111), *Phys. Rev.* **B84**, 155425 (2011).
 - ¹⁵ P. Merino, M. Svec, A. L. Pinardi, G. Otero, and J. A. Martn-Gago, Strain-Driven Moiré Superstructures of Epitaxial Graphene on Transition Metal Surfaces, *ACS Nano*, **5** 5627. (2011).
 - ¹⁶ K. L. Man and M. S. Altman, Small-angle lattice rotations in graphene on Ru(0001), *Phys. Rev.* **B84**, 235415 (2011). 28
 - ¹⁷ E. Starodub, A. Bostwick, L. Moreschini, S. Nie, F. El Gabaly, K. F. McCarty, and E. Rotenberg, In-plane orientation effects on the electronic structure, stability, and Raman scattering of monolayer graphene on Ir(111), *Phys. Rev.* **B83**, 125428 (2011), A. T. NDiaye, J. Coraux, T. N. Plasa, C. Busse, and T. Michely, In-plane orientation effects on the electronic structure, stability, and Raman

- scattering of monolayer graphene on Ir(111), *New J. Phys.* **10**, 043033 (2008).
- ¹⁸ P. Sutter, J. T. Sadowski, and E. Sutter, Graphene on Pt(111): Growth and substrate interaction, *Phys. Rev. B* **80**, 245411 (2009).
 - ¹⁹ L. Meng, R. Wu, L. Zhang, L. Li, S. Du, Y. Wang and H-J Gao, Multi-oriented moiré superstructures of graphene on Ir(111): experimental observations and theoretical models, *J. Phys.: Condens. Matter* **24**, 314214 (2012).
 - ²⁰ H. Hattab, A. T. NDiaye, D. Wall, G. Jnawali, J. Coraux, C. Busse, R. van Gastel, B. Poelsema, T. Michely, F.-J. Meyer zu Heringdorf, and M. Horn-von Hoegen, Growth temperature dependent graphene alignment on Ir(111)... *Appl. Phys. Lett.* **98**, 141903. (2011).
 - ²¹ Y. Murata, V. Petrova, B. B. Kappes, A. Ebnonnasir, I. Petrov, Y. Xie, C. V. Ciobanu, and S. Kodambaka, Moiré Superstructures of Graphene on Faceted Nickel Islands, *ACS Nano*, **4**, 6509. (2010).
 - ²² D. Martoccia, P. R. Willmott, T. Brugger, M. Bjorck, S. Gunther, C. M. Schleputz, A. Cervellino, S. A. Pauli, Graphene on Ru(0001): A 25×25 Supercell, *Phys. Rev. Lett.* **101**, 126102. (2008).
 - ²³ B. Borca, S. Barja, M. Garnica, M. Minniti, A. Politano, J. M Rodriguez-Garcia, J. J. Hinarejos, D. Farias, A. L Viquez de Parga, and Rodolfo Miranda, Electronic and geometric corrugation of periodically rippled, self-nanostructured graphene epitaxially grown on Ru(0001), *New Journal of Physics*, **12** 093018 (2010),
 - ²⁴ K. Hermann, Periodic overlayers and moiré patterns: theoretical studies of geometric properties., *J. Phys.: Condens. Matter* **24**, 314210 (2012).
 - ²⁵ S. K. Hämäläinen, M. P. Boneschanscher, P. H. Jacobse, I. Swart, K. Pussi, W. Moritz, J. Lahtinen, P. Liljeroth, J. Sainio, The Structure and Local Variations of the Graphene moiré on Ir(111), *Phys. Rev.* **B88**, 201406(R) (2013).
 - ²⁶ P. Süle, M. Szendrő, The classical molecular dynamics simulation of graphene on Ru(0001) using a fitted Tersoff interface potential, *Surf. Interf. Anal.*, **46**, 42 (2014).
 - ²⁷ D. Jiang, M.-H., Du and S. Dai, J. Chem. Phys. First principles study of the graphene/Ru(0001) interface, **130** 074705, (2009),
 - ²⁸ B. Wang, S. Günther, J. Wintterlin and M.-L. Bocquet, Periodicity, work function and reactivity of graphene on Ru(0001) from first principles, *New J. Phys.* **12**, 043041 (2010).
 - ²⁹ G. C. Abell, Empirical chemical pseudopotential theory of molecular and metallic bonding, *Phys. Rev.* **B31** 6184, (1985).
 - ³⁰ J. Tersoff, Empirical interatomic potential for carbon, with applications to amorphous carbon, *Phys. Rev. Lett.* **61**, 2879. (1988), Modeling solid-state chemistry: Interatomic potentials for multicomponent systems, *Phys. Rev.* **B39**, 5566. (1989), D. W. Brenner, Empirical potential for hydrocarbons for use in simulating the chemical vapor deposition of diamond films, *Phys. Rev.* **B42**, 9458. (1990).
 - ³¹ S. Marchini, S. Günther, J. Wintterlin, Scanning tunneling microscopy of graphene on Ru (0001), *Phys. Rev.* **B76**, 075429 (2007).
 - ³² A. T N'Diaye, J. Coraux, T. N. Plasa, C. Busse and T. Michely, Structure of epitaxial graphene on Ir(111), *New J. of Phys.* **10**, 043033 (2008).
 - ³³ E. N. Voloshina, Yu. S. Dedkov, S. Torbrugge, A. Thissen, M. Fonin, Graphene on Rh(111): Scanning tunneling and atomic force microscopies studies E. N. Voloshina, Yu. S. Dedkov, S. Torbrugge, A. Thissen, M. Fonin, *Appl. Phys. Lett.*, **100**, 241606 (2012).
 - ³⁴ F. Varchon, P. Mallet, L. Magaud, and J.-Y. Veuillen, Rotational disorder in few-layer graphene films on : A scanning tunneling microscopy study, *Phys. Rev.* **B77**, 165415 (2008).
 - ³⁵ W. Gannett, A. Zettl, and M. F. Crommie, R. Decker, Y. Wang, V. W. Brar, W. Regan, H.-Z. Tsai, Q. Wu, *et al.* Local Electronic Properties of Graphene on a BN Substrate via Scanning Tunneling Microscopy, *Nano Lett.* **11**, 2291 (2011).
 - ³⁶ E. N. Voloshina, E. Fertitta, A. Garhofer, F. Mittendorfer, M. Fonin, A. Thissen, and Yu. S. Dedkova, Electronic structure and imaging contrast of graphene moiré on metals *Sci. Rep.*, **3**, 1072 (2013).
 - ³⁷ S. J. Plimpton, *Fast Parallel Algorithms for Short-Range Molecular Dynamics*, *J. Comp. Phys.*, **117**, 1-19 (1995), see also the URL <http://lammps.sandia.gov>.
 - ³⁸ A. Stukowski, Visualization and analysis of atomistic simulation data with OVITO the Open Visualization Tool, *Modell. and Simul. in Mater. Sci. and Eng.*, **18**, 015012 (2010).
 - ³⁹ P. Süle, Ion-erosion induced surface nanoporosity and nanotopography on Si, *J. Chem. Phys.*, **134**, 244706 (2011).
 - ⁴⁰ S. J. Stuart, A. B. Tutein, J. A. Harrison, A reactive potential for hydrocarbons with intermolecular interactions *J. Chem. Phys.* **112**, 6472. (2000).
 - ⁴¹ H.W. Sheng, M.J. Kramer, A. Cadien, T. Fujita and M.W., Highly-optimized EAM potentials for 14 fcc metals, *PRB* **83**, 134118 (2011).
 - ⁴² J. Klimes, D. R. Bowler and A. Michaelides, Chemical accuracy for the van der Waals density functional, *J. Phys.: Condens. Matter*, **22**, 022201. (2009).
 - ⁴³ E. Artacho, E. Anglada, O. Dieguez, J. D. Gale, A. Garcia, J. Junquera, R. M. Martin, P. Ordejn, J. M. Pruneda, D. Sanchez-Portal and J. M. Soler, The SIESTA method; developments and applicability, *J. Phys.: Condens. Matter* **20**, 064208 (2008).
 - ⁴⁴ M. Szendrő, P. Süle, code potfit: *parameter fitting of the Tersoff potential using ab initio DFT data base* (2013).
 - ⁴⁵ P. Süle, M. Szendrő, Time-lapsed graphene moiré superlattice on Cu(111), eprint: arXiv:1402.4692
 - ⁴⁶ User's Guide, SIESTA 3.1, trunk-367, www.icmab.es/siesta
 - ⁴⁷ M. Birowska, K. Milowska and J.A. Majewski, Van Der Waals Density Functionals for Graphene Layers and Graphite, *Acta Physica Polonica A*, **120**, 845 (2011).
 - ⁴⁸ M. A. Akhukov, A. Fasolino, I. Y. N. Gornostyrev, and M. I. Katsnelson, Dangling bonds and magnetism of grain boundaries in graphene, *Phys. Rev.* **B85**, 115407 (2012).
 - ⁴⁹ E. Loginova, S. Nie, K. Thürmer, N. C. Bartelt, and K. F. McCarty, Defects of graphene on Ir(111): Rotational domains and ridges *Phys. Rev.* **B80**, 085430. (2009).
 - ⁵⁰ L. Tapasztó, T. Dumitric, S. Jin Kim, P. Nemes-Incze, C. Hwang, and L. P. Biró, Breakdown of continuum mechanics for nanometre-wavelength rippling of graphene, *Nature Physics*, **8**, 739 (2012).
 - ⁵¹ T. Yoon, W. C. Shin, T. Y. Kim, J. H. Mun, T.-S. Kim, B. J. Cho, Direct Measurement of Adhesion Energy of Monolayer Graphene As-Grown on Copper and Its Application to Renewable Transfer Process, *Nano Lett.* **12**, 1448. (2012)
 - ⁵² T. Olsen, and K. S. Thygesen, Random phase approxi-

mation applied to solids, molecules, and graphene-metal interfaces: From van der Waals to covalent bonding, Phys. Rev. **B87**, 075111. (2013).

⁵³ S. P. Koenig, N. G. Boddeti, M. L. Dunn, J. S. Bunch,

Ultra-strong adhesion of graphene membranes, Nat. Nanotech. **6**, 543546 (2011).